Nanoscale

Accepted Manuscript

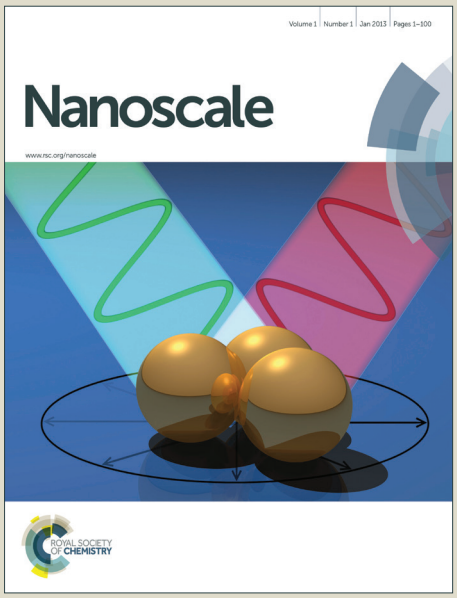

Nanoscale RSCPublishing

ARTICLE

Gold Nanostar Substrates for SERS-based Chemical Sensing in the Femtomolar Regime

Cite this: DOI: 10.1039/x0xx00000x

A. S. D. S Indrasekara,[a] S. Meyers,[a] S. Shubeita,[c] L. C. Feldman,[a,b,c] T. Gustafsson[c] and L. Fabris[a,b]

Received 00th January 2012,
Accepted 00th January 2012

DOI: 10.1039/x0xx00000x

www.rsc.org/

We report a novel approach for fabricating gold nanostar-functionalized substrates for highly sensitive surface enhanced Raman spectroscopy (SERS)-based chemical sensing. Gold nanostars immobilized on a gold substrate via a Raman silent organic tether serve as the SERS substrate, and facilitate the chemical sensing of analytes that can either be chemisorbed or physisorbed on the nanostars. Our SERS substrates are capable of detecting chemisorbed 4-mercaptobenzoic acid at a concentration as low as 10 fM with a reproducible SERS enhancement factor of 10^9, and enable the semi-quantitative multiplexed identification of analytes from mixtures in which they have been dissolved in variable stoichiometry. Most importantly, they afford the detection of physisorbed analytes, such as crystal violet, with excellent signal-to-noise ratio, hence serving as versatile platform for the chemical identification of in principle any molecular analyte. These characteristics make a strong case for the use of our nanostar-based SERS substrate in practical chemical sensing applications.

Introduction

Raman spectroscopy is a valuable analytical tool that employs characteristic vibrational patterns for the identification of molecules, but its direct implementation as a chemical sensing technique is limited due to the low scattering cross section of most Raman active molecules, which leads to low sensitivity. [1] This limitation has been overcome by the discovery of surface enhanced Raman scattering (SERS), which increases the intensity of Raman signals by leveraging the inherent and unique properties of plasmonic nanoparticles leading to improved detection limits. [1-3] The interaction of electromagnetic radiation with the oscillating cloud of conduction electrons of plasmonic nanoparticles results in electromagnetic energy confinement around the nanoparticles. By placing a Raman active molecule on or in close proximity to the nanoparticles, and within the confined electromagnetic field, it is possible to obtain significant Raman signal amplification. This phenomenon is known as SERS. [1, 3-5]

The design and fabrication of plasmonic nanoparticles to sustain high electromagnetic field enhancements for SERS have become a field of interest in the analytical research community due to the high demand of ultrasensitive substrates for the detection of environmental pollutants, toxic industrial waste, and chemical warfare, to name a few. In SERS-based experiments, when a Raman active molecule (SERS reporter) is attached to a plasmonic nanoparticles (SERS substrate), its Raman signal is boosted on average by about 5-6 orders of magnitude, with peaks of 8-10 orders of magnitude in non ensemble-averaged systems. [6-9] It has been established that SERS signals can also be intensified via assembly of the plasmonic NPs into dimers and small clusters, where the local electromagnetic field enhancement increases by up to a value of 10^8-10^{10} at the junction between nanoparticles, which is also known as "SERS hot spot". [8, 10-12] In addition, high confinement of the electromagnetic energy has also been reported to be present at the sharp edges or tips of anisotropic nanoparticles such as nanorods, nanocubes, and nanoprisms, which have also been widely studied and reported in literature as superior SERS substrates. [13, 14] Recently, star-shaped gold nanoparticles (spherical core structures with protruding sharp tips) have emerged as excellent SERS substrates, where extraordinary field confinement and enhancement can be observed at the acute tips, that can thus act as excellent "hot spots". [15-18] The optical properties of nanostars have also been found to be strongly dependent on the morphology of the protruding tips. [16, 19] This excellent structure-optical property relationship in gold nanostars has been exploited to design substrates for chemical- as well as bio-detection. [20-26]

Top-down and bottom-up techniques have been equally utilized for the fabrication of SERS substrates. [27, 28] Many elegant nanoparticle substrates have been presented with reproducible large-scale periodic arrays by using, for example, electron beam lithography and focused-ion beam lithography. [27, 29] However, the implementation of top-down methods is limited by the high fabrication cost and the constraints in the inter-nanoparticle space tunability necessary to achieve maximum field enhancements. [30] These limitations can be circumvented by bottom-up procedures that are much cheaper and offer flexibility in controlling the inter-nanoparticle spacing, particularly for nanoparticle-assembly-guided SERS substrates, easily reaching inter-nanoparticle separations as low as 1 nm. Bottom-up approaches also permit the use of anisotropic NPs, like gold nanostars and nanorods, which exhibit excellent

plasmonic properties with size tunability. [13, 31, 32] Similar to the top-down methods, SERS platforms prepared from the bottom-up can and should be well characterized for quantitative data acquisition, and designed with high reliability and reproducibility by careful and controlled fabrication practices. Successful implementations of these advantageous features are evident in the variety of emerging bottom-up designed SERS substrates with superior SERS enhancement. [20, 28, 33]

In literature, most of the nanoparticle fabrication methods for SERS-based chemical sensing applications have followed the "sandwich architecture", where a narrow gap between nanoparticles or nanoparticles and a plasmonic film is created, to take advantage of the quantum confinement effect. [19] Liz-Marzan *et al*. have designed substrates by a bottom-up approach where dithiolated analyte molecules are sandwiched between a gold film and gold nanostars, and enable zeptomolar sensitivity in the detection of 1-naphthalenedithiol. [20] However, in practice, this approach limits its use only to dithiolated analytes. A modified version of this approach was later reported by the same group for the detection of non-functionalized analytes with limits of detection up to 10^{-5} M. [22] The authors reported that the SERS spectrum for such analytes could only be acquired when they were positioned exactly at the junction between the nanostar tips and the gold thin film. [22] This criterion however would be hard to implement in ultrasensitive detection regimes, thus limiting their widespread use. Not only star-shaped nanoparticles but also other anisotropic nanoparticles, fabricated to give rise to quantum confinement effects, have been used in the literature for SERS-based chemical detection. [34, 35] Even though these approaches have been able to address the detection of different types of analytes, several improvements are still needed in the engineering of SERS substrates, particularly for ultrasensitive detection of non-functionalized analytes.

Below, we present a novel and alternative construct of a gold nanostar-based SERS substrate, which offers flexible detection of analytes regardless of their chemical affinity towards gold nanoparticles, high sensitivity, reproducibility, and the possibility to easily implement it for multiplexed detection. Smooth gold thin films deposited on Si substrates are functionalized with Raman silent, primary amine-terminated, short alkanethiols that are used as tethers to anchor the ascorbic acid-capped gold nanostars. Our approach does not involve externally induced quantum confinement effects (i.e. the creation of "hot spots" via nanostructure assembly); instead, the analytes directly interact with the nanoparticles and therefore the observed SERS enhancement can be directly linked to the SERS properties of the nanoparticle itself. In this article, we highlight the applicability of our SERS substrate for flexible (i.e. not limited by the pendant functional groups of the analyte), multiplexed, and reliable semi-quantitative SERS-based chemical detection.

Experimental Section

Materials

Hydrogen tetrachloroaurate ($HAuCl_4 \cdot 3H_2O$), trisodium citrate, ascorbic acid, silver nitrate, 6-aminohexane-1-thiol (AHT), hexane-1-thiol (HT), 4-mercaptobenzoic acid (4-MBA), 4-aminothiophenol (ATP), 5-phenyl-1,3,4-oxadiazole-2-thiol (PODT), dibenzene-4-thiol (DBT), and crystal violet (CV) were purchased from Sigma Aldrich. Naphthalene-2,6-dithiol (NP) was purchased from Matrix Scientific. Si (100) wafers were purchased from University Wafers Inc. Ultrapure MiliQ water was used for all the syntheses. All the glassware was cleaned with aqua regia followed by MiliQ water and air-dried before use.

Nanoparticle Synthesis

Gold nanostars were synthesized according to a modified version of the surfactant-free nanostar synthesis described by Vo-Dinh *et al*. [21] Briefly, 20 µL of 1 N HCl and 6.25 µL of 12 nm citrate capped spheres (absorbance, A = 2.81) were added to 10 mL of 1 mM $HAuCl_4$ solution and mixed thoroughly by stirring. Then 200 µL of 100 mM ascorbic acid and 400 µL of 3 mM $AgNO_3$ were simultaneously added to the above mixture, gently stirred for 7 min, and purified by centrifugation at 3000 g for 15 min. As purified gold nanostars (NS-1) were resuspended in 10 mL of MiliQ water and refrigerated until further use. Gold nanostars with different plasmonic properties were synthesized by changing the seed volume and concentration of $HAuCl_4$. In particular, the same procedure was followed with 25 µL of seeds to synthesize NS-2, and with 10 mL of 0.4 mM $HAuCl_4$ to synthesize NS-3. The syntheses of ~36 nm (SP-36) and ~130 nm (SP-130) in diameter citrate capped gold nanospheres were carried out according to the protocols published by Bastus *et al*. [36]

Immobilization of nanoparticles on substrates

Si substrates of 0.5 × 0.5 cm^2 surface area were cleaned with methanol, acetone, water, and hydrofluoric acid in the given order. Air-dried Si substrates were then sputter coated with a smooth 60 nm thick layer of gold. The gold-coated Si substrates were then immersed in 4 mM ethanolic solution of AHT for 24 hrs to form a self-assembled monolayer (SAM) followed by thorough rinsing with ethanol and air-drying. Next, the smooth gold substrates were incubated with 1mM HT (blocking agent) for 24 hrs, rinsed with ethanol and air-dried. Any remaining empty sites on the gold substrates will be occupied by HT thereby preventing non-specific binding of analyte molecules onto the bare gold substrate. As prepared SAMs of AHT were then incubated with colloidal suspensions of gold nanoparticles for 48 hrs followed by rinsing with MiliQ water. Samples were prepared by using varying concentrations of gold nanoparticles (500 µL of 0.5 nM, 1.0 nM, and 3 nM) in order to coat the substrates with varying nanoparticle densities. Gold nanostars and nanospheres were both used for substrate preparation. The thiol moiety of AHT covalently binds to the gold substrate while its pendant primary amine group covalently binds to the nanoparticles. As prepared gold nanoparticle-coated substrates were then incubated with varying concentrations of analyte molecules for 24 hrs followed by thorough rising with ethanol. Ethanolic solutions of 4-MBA (100 µM to 10 fM), ethanolic solutions of CV (100 µM to 1 pM), and a mixture of ethanolic 4-MBA and DBT in THF (100 µM to 1 pM) were used as the analytes of interest. For 3-plex and 4-plex chemical sensing experiments, 1 µM ethanolic solutions of the analytes of interest were used on NS-1 substrates. All the samples were air-dried before analysis.

Characterization

The UV-vis spectra were recorded on a Nanodrop 3000 spectrometer (Thermo Scientific). The morphology of the nanoparticles was evaluated by using a Topcon 002B transmission electron microscope, and size information was extracted using the Image J software. Nanoparticle substrates were characterized for surface coverage and aggregation by an

ORION™ Helium ion microscope (Carl Zeiss SMT), and an atomic force microscope (Digital instrument nanoscope iii).
All the Raman and SERS spectra of analyte solutions and nanoparticle substrates were obtained using a Reinshaw inVia Raman microscope. The SERS spectra for gold nanostar substrates were obtained using a 785 nm diode laser excitation (166 μW, spot diameter 1 mm) while 633 nm HeNe laser excitation (492 μW, spot diameter 1 mm) was used for nanosphere-coated substrates with single accumulation for 10 s acquisition time under a 50X objective. SERS spectra and intensities presented here are the averages of five baseline-corrected measurements obtained at random places on the samples. SERS intensities of the samples are normalized to the response of an internal reference (i.e. the intensity of Si peak at 512 cm^{-1}) and reported here as I_{SERS}/I_{Ref}. For SERS mapping, 20 × 20 μm^2 areas on the samples were raster-scanned at 2 μm step size under the same acquisition conditions reported above.

Results and Discussion

Nanoparticle Characterization

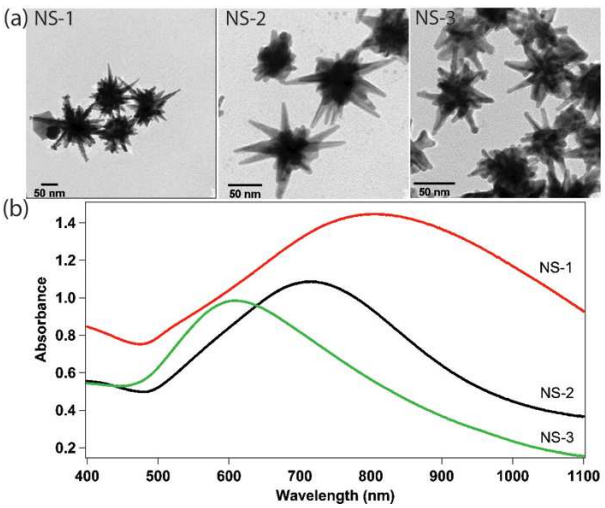

Fig. 1 Gold nanostars of varying tip morphology and spectral properties: Tip morphology and plasmonic properties are directly correlated. (a) Transmission electron microscopy images, and (b) UV-visible spectra of gold nanostars.

Gold nanostars (NS) with plasmon peak maxima at 830 nm (NS-1), 720 nm (NS-2), and 620 nm (NS-3) were synthesized and analyzed to understand the effect of NS morphology on SERS enhancement factors (EF) and thereby on the detection sensitivity (Fig. 1). Among these nanostars, there is a distinct difference in the number of tips per nanoparticle and the sharpness of the tips, where NS-1 possesses more tips with a higher sharpness while NS-3 has relatively shorter and less sharp tips. Our gold nanostar synthesis is a modified version of the original protocol by Vo-Dinh *et.al.* As opposed to the original protocol, our nanoparticles are aged for 7-10 min at room temperature before purification by centrifugation.[21] We believe that nanoparticle aging might provide extended time for the anisotropic growth of the protrusions extending from the spherical core, hence leading to longer and sharper spikes (with tip curvature of 3-5 nm) compared to what one can expect employing the original protocol. The spherical core of the NS is equivalent to a sphere of 36 ± 3 nm in diameter while the outer diameter of the NS (that is the imaginary sphere that can be drawn by connecting the outermost atoms on the tips) equals 130 ± 6 nm. Therefore gold nanospheres of 36 nm and 130 nm in diameter were synthesized and analyzed to compare the SERS EF and detection limits of gold nanospheres to those of NS (Fig. S1).

Fabrication of gold nanoparticle substrates

A schematic representation of the gold nanoparticle substrates is shown in Scheme 1. A smooth (i.e not SERS enhancing) gold thin film sputtered on a Si substrate was functionalized with 6-aminohexanethiol (AHT) by exploiting the higher affinity of thiol moieties toward gold surfaces. The substrates were then treated with hexane-1-thiol (HT) in order to block remaining binding sites (if present) on the substrates. Blocking the surface prevents non-specific interactions between analyte molecules and the Au substrate, which would interfere with the SERS analysis. The pendant $-NH_2$ group of AHT was then used to immobilize nanoparticles onto the substrate via Au-N covalent bonding. The affinity of N for Au is lower than that of S, nonetheless this type of chemistry can be employed to effectively bind nanoparticles to the substrates. As-prepared nanoparticle substrates were incubated with varying concentrations of analytes to evaluate the lowest detection limits and the SERS EF for the nanoparticle substrates. A thiolated aromatic molecule that chemisorbs to Au nanoparticles, namely, 4-mercaptobenzoic acid (MBA) and the non-thiolated crystal violet dye (CV) that adsorbs to Au nanoparticles, were used as the analytes of interest to evaluate the performance of our substrate on analytes of different chemical structure. The multiplexing capability of our NS substrates was also qualitatively studied using mixtures of MBA, 4-aminothiophenol (ATP), 5-phenyl-1,3,4-oxadiazole-2-thiol (PODT) and Naphthalene-2,6-dithiol (Nap) at varying molar ratios (both 3-plex and 4-plex experiments), while a mixture MBA and ATP was employed for quantitative multiplexed detection. The effect of the substrate surface coverage on the performance of the sensor was studied by using substrates prepared with different nanoparticle concentrations (0.5 nM, 1 nM, and 3 nM, for both stars and spheres).

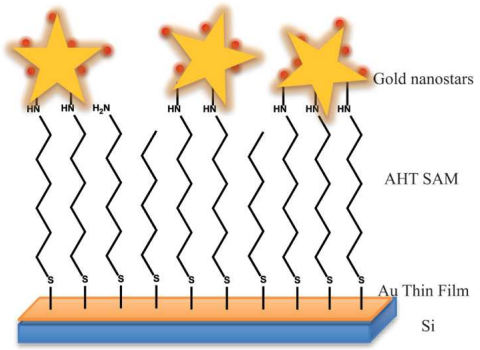

Scheme 1. Schematic representation of the nanoparticle substrate used for SERS-based chemical detection. A self-assembled monolayer of 6-aminohexane-1thiol (AHT) is used to immobilize the gold nanoparticles on a smooth gold-coated Si wafer. Hexane-1-thiol (HT) is used as the blocking agent. The solid red circles represent the analyte molecules of interest that are chemisorbed or physisorbed onto the gold nanoparticles. Drawing not to scale.

Atomic force micrographs (AFM) of Au thin films on Si substrates prior to nanoparticle deposition provide evidence of a smooth Au surface (RMS = 0.282 nm) (see Fig. S2). The presence of a smooth Au surface is important in order to

eliminate any SERS enhancement due to the surface roughness that could interfere with the analyte detection. AFM images of nanoparticle-coated substrates also provide conclusive evidence of the immobilization of the nanoparticles of interests on the substrates (Fig. 2a and Fig. S2a). Helium ion microscopy (HIM) images were acquired to calculate the nanoparticle surface coverage that is the density of nanoparticles present in a given field of view (Fig. 2b and Fig S2b). 3 nM SP-130 substrates present a surface density of 150 spheres / μm^2 with 30% particle aggregation while 3 nM NS-1 substrates have an average surface density of 110 stars/ μm^2 with 20% aggregates. The micrographs also show that the nanostar surface coverage increases as the concentration of the nanoparticle suspension increases.

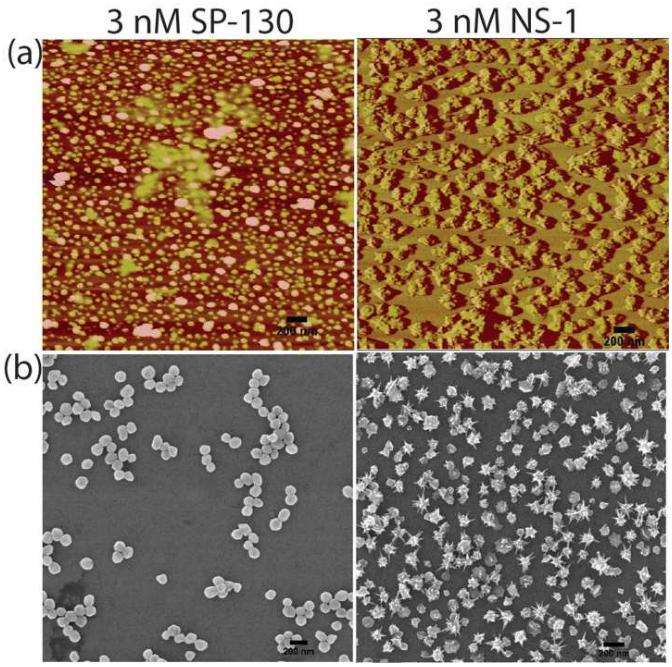

Fig. 2 Surface characterization of the gold nanoparticle substrates used for SERS-based chemical sensing. (a) Atomic force micrographs (Image size: 3×3 µm), and (b) Helium ion micrographs (HIM) of 3 nM SP-130 and 3 nM NS-1 nanoparticle substrates. 3 nM NS-1 substrate (RMS $_{[Rq]}$ = 39.00 nm) shows 110 particles/μm^2 surface coverage with 20 % aggregation while 3nM SP-130 substrate (RMS $_{[Rq]}$ = 15.58 nm) has a surface coverage of 150 particles/μm^2 with 30 % particle aggregation.

SERS-based detection of 4-MBA on gold nanostar substrates

The applicability of the gold nanostar substrates for quantitative chemical detection was demonstrated by SERS analysis of MBA as the model molecule. MBA is a Raman active molecule with a relatively low scattering cross-section, which can chemisorb to Au nanoparticles via its pendant thiol moiety as well as through π system interaction. [37, 38] SERS analysis is also used (a) to determine the lowest detection limit that can be achieved using the nanostar substrate, and (b) to compare the effectiveness and SERS EF of nanostars over nanospheres for SERS-based chemical sensing (proof-of-concept experimentation).

For comparison purposes, the Raman spectra of analyte solutions and blank substrate (NS-1) were collected under the same conditions (Fig. 3). The blank substrate by itself displays two weak peaks at 1123 cm^{-1} and 1163 cm^{-1}, and a broad peak ranging from 1450-1600 cm^{-1} with very low intensities compared to that of the analytes (about 20–fold weaker). These peaks can be attributed to the residual ascorbic acid molecules that remain on gold nanostars. [39] However, these background peaks of weak intensity do not interfere with the detection of the analyte molecules, even at low analyte concentrations (Fig 3).

Fig. 3a shows the Raman spectrum of an ethanolic solution of 50 mM MBA, and the SERS spectrum of MBA on NS-1 substrates (Fig. 5). The characteristic peaks associated with ring breathing modes at 1077 cm^{-1} and 1582 cm^{-1} were identified along with the band at 830 cm^{-1} and 1421 cm^{-1} corresponding to deformation and stretching vibrations of carboxylate groups. For SERS analysis, the NP substrates were incubated with varying concentrations of ethanolic MBA from 1 mM to 10 fM, and the SERS intensity at 1077 cm^{-1} was recorded.

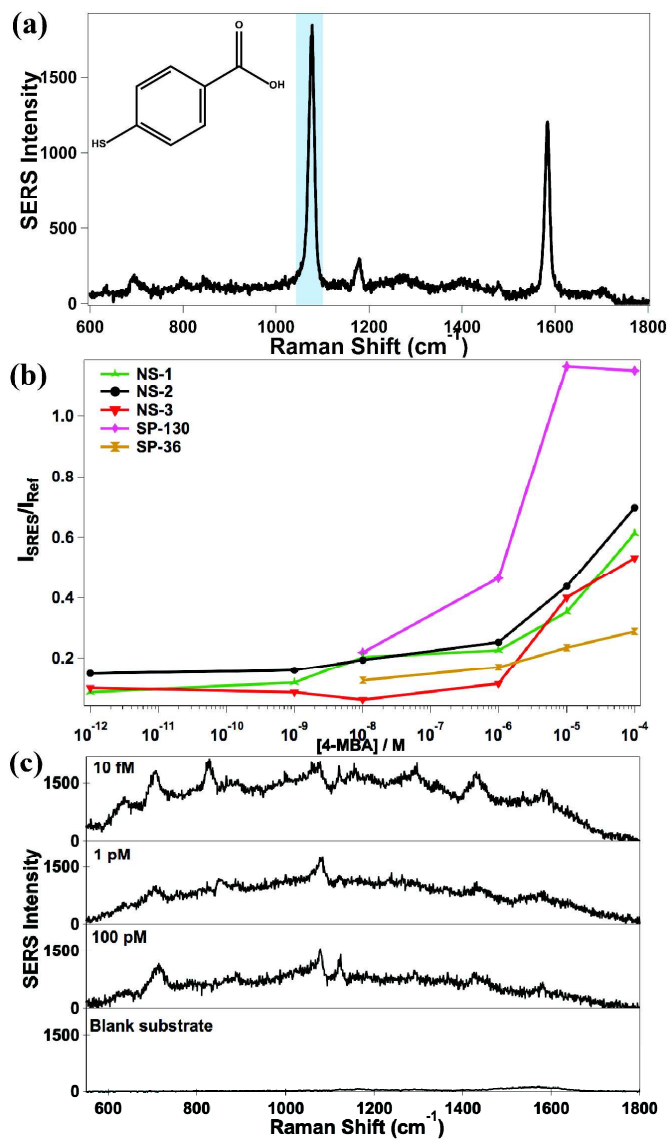

Fig. 3 Quantitative SERS analysis is facilitated by our SERS substrates, and lower SERS detection limits are provided by substrates functionalized with nanostar over nanospheres. (a) Raman spectrum of 50 mM ethanolic MBA solution, (b) variation of the SERS response for gold nanostar (NS) and nanospheres (SP) substrates as a function of the concentration of MBA, and (c) SERS spectra for the blank NS-1 substrate and 4-MBA in the lower concentration regime on 3 nM NS-1 substrates. The characteristic SERS peaks of MBA at 1077 cm^{-1} and 1583 cm^{-1} can still be clearly identified in the range of 100 pM to 10 fM. The plotted

SERS responses were collected at 1077 cm^{-1} under 785 nm laser (166 μW) for NS substrates, and 633 nm laser (492 μW) for nanospheres substrates. Raman and SERS responses for the Si peak at 512 cm^{-1} were used as the internal reference.

Both nanospheres and nanostar substrates show a nearly linear trend between the SERS response and the concentration of MBA, where the SERS response decreases as the concentration of MBA decreases (Fig. 3b). It should be noted that the trend line was drawn only to guide the reader towards the concentration dependence of SERS response, and it is not meant to be an interpolation. This linear trend is more prominent at lower analyte concentrations (below 10 μM), which could be attributed to the presence of a single monolayer of analyte molecules atop the nanoparticles (instead of several monolayers that could be generated at higher concentrations). These data provide a strong evidence to support the use of our SERS substrates in quantitative SERS-based chemical sensing. The SERS signature of MBA was detectable at 1 pM for all the NS samples. On the other hand, the lowest detection limit for MBA on citrate-capped gold nanospheres of 36 nm in diameter (SP-36) and 130 nm in diameter (SP-130) substrates was limited to 10 nM under the same experimental conditions. This observation supports the concept that a higher SERS enhancement is exhibited by nanoparticles with sharp tips over their spherical counterparts (proof-of-concept experimentation). [22] For NS-1 substrates, the most sensitive of the set, SERS analysis at a much lower concentration regime was carried out. It revealed that 10 fM of MBA is the lowest SERS detection limit achievable with this substrate with a good signal-to-noise ratio (S/N =3.8), which is equivalent to 900 molecules (see below for a detailed calculation) sampled by the laser beam spot (Figs. 3c and S4). As the concentration of MBA decreases, we also observed that the SERS responses were localized only at certain locations but not all over the substrate, which has also been reported in literature. [22] Interestingly, as the probing concentration of MBA decreases below 100 nM, it can be noticed that the relative intensity of the SERS peak at 1077 cm^{-1} decreases while the peak at 715 cm^{-1} increases. The ring-breathing mode at 1077 cm^{-1} is a characteristic of MBA when it is bonded to Au through S in a nearly upright position. [38] The peak at 715 cm^{-1} arises due to the out-of-plane C-C-C bending mode, which appears when the molecule is sitting parallel to the Au surface. [38] This observation suggests that as the analyte concentration decreases, the orientation of the analyte with respect to the Au surface changes so as to maximize the molecular interaction, which is reflected by peak pattern changes in the SERS spectra, hence rendering our substrate potentially interesting for the mechanistic charaterization of the interactions between nanostructures and molecularly- or biomolecularly-relevant analytes.[40]

The SERS enhancement of MBA on the nanoparticle substrates was calculated by considering the intensity at 1077 cm^{-1}, and using the following equation: [4]

$$EF = [I_{SERS}] / [I_{Raman}] \times [N_{Raman}] / [N_{SERS}]$$

The SERS intensity (I_{SERS}) at 1 pM MBA for NS substrates and 10 nM 4-MBA for nanospheres substrates was considered for SERS EF calculations. Since a patchy distribution of SERS signal was observed at the lowest detectable MBA concentration on NS substrates (10 fM), we decided to consider 1 pM MBA-treated NS substrates for accurate estimation of EF, where a monolayer coverage of analytes over nanoparticles can be ensured. The average Raman intensity for 50 mM ethanolic MBA was considered for I_{Raman}. N_{Raman} was calculated as the number of MBA molecules present in the laser spot size. In order to calculate N_{SERS} within the laser spot size, it was assumed that a monolayer of MBA molecules exists all over the SERS substrate. Knowing the analyte surface coverage and the surface area irradiated by the laser excitation, the number of probed MBA molecules was calculated using the following equation:

N_{SERS} = (Molar Surface coverage of the analyte × Avogadro number × lasers spot size)

The SERS EFs for MBA on the test substrates are tabulated in the Table 1. According to the calculations, NS substrates showed SERS enhancements that are 4 orders of magnitude higher than those calculated for substrates coated by Au nanospheres of corresponding size. This can be mainly attributed to morphological differences, where the sharp tips of star-shaped nanoparticles act as SERS "hot spots". However, in this experiment, we did not address all the tips individually with suitably polarized light as we assumed that the analyte molecules are distributed all over the nanostar surface rather than being concentrated at the tip. It should also be noted that our approach in designing SERS substrates did not utilize the external "quantum confinement effect" and therefore the observed SERS EF can be correlated to the particle morphology itself. Under the given conditions, the calculated SERS EF for nanostar substrates, 10^9, is very reasonable and close to theoretical predictions [41], and it is anticipated that even larger SERS EFs could be achieved under optimized conditions. Under 785 nm laser excitation, the SERS EF for our NS substrates is 3-4 orders of magnitude higher than the values reported by Yuan *et. al* (4×10^5) and Lee *et. al* (2.7×10^6) for gold nanostars. [26, 42] This can be attributed to the presence of much sharper tips, which was achieved by modifications in the synthetic protocols, and owing to the absence of polymers or other thick surfactant coatings on our nanostars.

Table 1 Calculated SERS EF for 4-MBA on gold nanoparticle substrates.

Substrate	Average SERS EF
3 nM NS-1	4.9×10^9
3 nM NS-2	1.6×10^9
3 nM NS-3	5.3×10^8
3 nM SP-36	6.7×10^4
3 nM SP-130	1.2×10^5

The observed difference in SERS EF for different nanostars explains the importance, besides the morphology, of the laser excitation source in achieving the maximum electromagnetic enhancement. It is well known that having plasmon resonance peaks overlapping with the laser excitation wavelength leads to maximized surface plasmon responses and can thereby yield the maximum SERS EF that can be achieved for a given nanoparticle. [43] The plasmon peak for NS-1 is located at around 800 nm (see Fig. 1b), which is very close to the laser excitation wavelength (785 nm). This resonance gives a significant contribution to the observed EF for NS-1, in comparison to what seen for NS-3 where the laser excitation is slightly off-resonance with the plasmon peak located at 630 nm.

Fig. S3 shows the variation of SERS response for MBA as a function of the NS-1 density on the SERS substrate. Regardless of the NS-1 densities on the substrates (28 particles/μm^2 vs. 110 particle/μm^2), the SERS EF lies within the same order of magnitude (10^9). This observation suggests that, in the absence of major clustering and aggregation, the morphology of the

nanoparticles plays a more important role in the SERS effect than the surface coverage levels herein considered do.

In practice, unlike MBA, most analyte molecules do not possess thiol moieties that can facilitate chemical interactions with gold nanoparticle substrates. In order to understand the capability of our substrates to detect physisorbed, rather than chemisorbed, analyte molecules, a set of experiments was carried out with 3 nM NS-1 substrates for crystal violet (CV) as the model analyte. The adsorption of non-functionalized aromatic molecules onto gold substrates through their π system has been shown experimentally.[22,40] Therefore we assumed that CV can interact with Au NPs through its highly conjugated π system, which is weaker in comparison to the chemical bonding that occurs with MBA. Aqueous solutions of CV at neutral pH show a maximum absorption at 590 nm. [44] Therefore, in order to avoid the resonance Raman effect and to accurately estimate the signal enhancement, all the SERS measurements for CV samples were carried out under 785 nm laser excitation. Even without chemical bonding between nanostars and CV, NS-1 substrates were able to detect CV at a concentration as low as 1 pM with a SERS EF of 1.1×10^8 (Fig. 4). This suggests the applicability of our nanostar-based SERS substrates for analyte molecules that lack chemical affinity towards gold. These observations also explain the importance of considering the mode of interaction of the analyte with the nanoparticle in claiming the SERS EF for a given nanoparticle substrate.

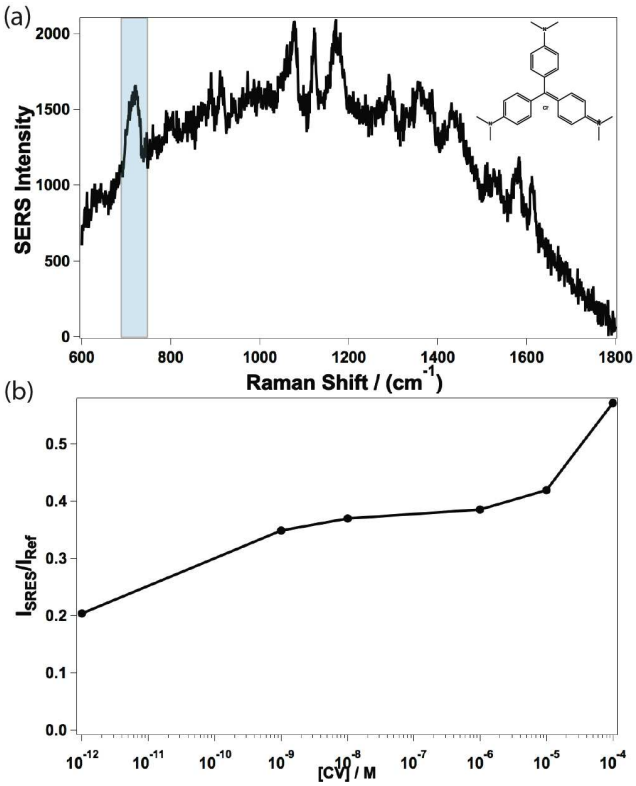

Fig. 4 The SERS response of crystal violet (CV) molecules on NS-1 substrates shows a linear concentration dependence. (a) SERS spectrum of 10^{-12} M CV on 3 nM NS-1 substrate. (b) The variation of the SERS intensity as a function of CV concentration. The plotted SERS responses were collected for the 795 cm^{-1} peak under 785 nm laser excitation (166 μW). Raman and SERS responses for the Si peak at 512 cm^{-1} were used as the internal reference.

Multiplexed chemical detection on gold nanostar substrate

To demonstrate the multiplexing chemical sensing potential of the NS-based SERS substrates, mixtures of three (3-plex) and four (4-plex) analytes with similar chemical signature at different molar proportions were assessed. In particular, NS-1 substrates were treated with varying molar ratios of 10^{-6} M analyte solutions. Then, the presence of each analyte in multiplexed samples was identified by their characteristic and dominant peaks in the SERS spectra. The SERS spectra for each analyte (MBA, ATP, PODT, and NP) and their spectral signatures are shown in Fig. 5 and Table S1 respectively. Fig. 6 shows the SERS spectra of 3-plex and 4-plex samples where the key peaks for individual analyte molecule are labelled with different symbols that can be used for identification purposes.

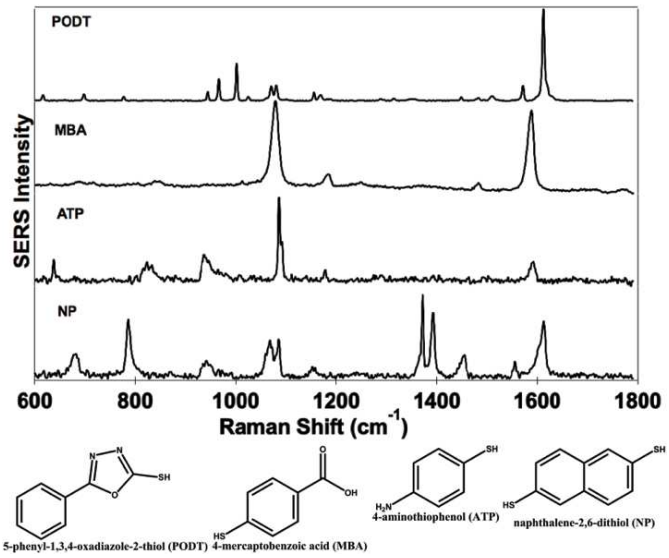

Fig. 5 SERS spectra of individual analytes used for multiplexed chemical sensing proof-of-concept analysis on 3 nM NS-1 substrates (785 nm laser excitation, 10 s exposure, 1 accumulation).

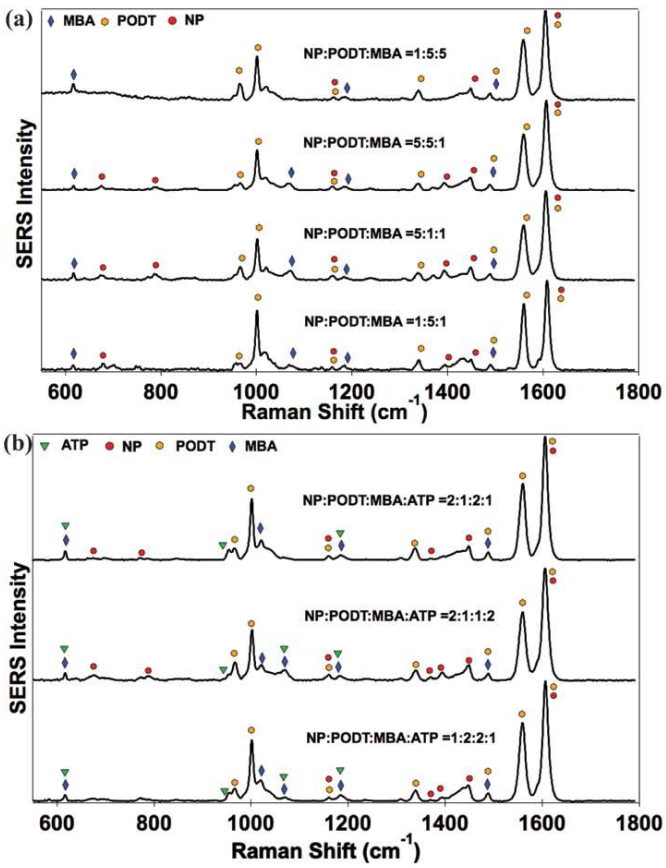

Fig. 6 SERS multiplexing can be achieved on gold nanostar substrates. (a) SERS spectra show the characteristic peaks for analytes in 3-plex, and (b) 4-plex chemical sensing experiments for 10^{-6} M analytes on 3 nM NS-1 substrate. SERS spectra were collected under 785 nm laser excitation (1 accumulation, 10 s exposure).

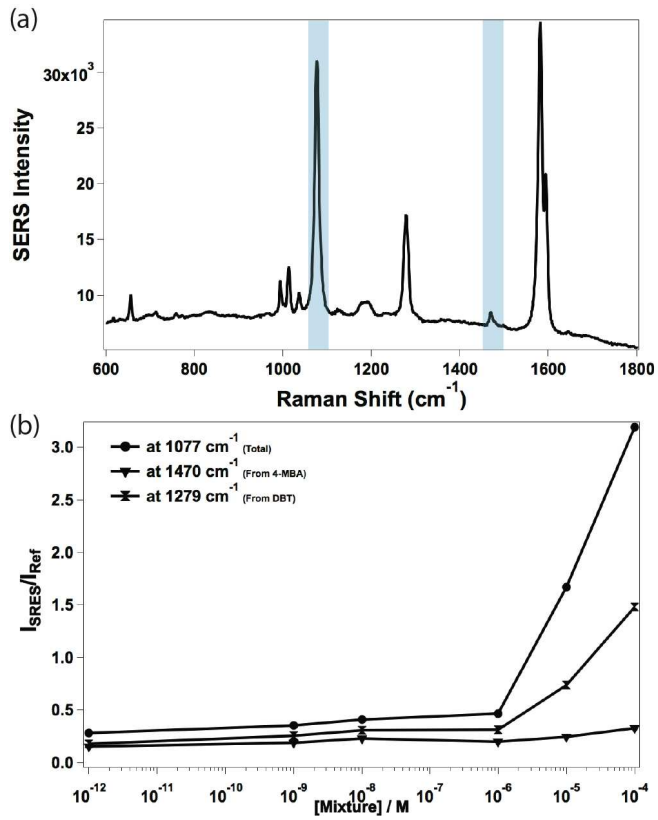

Fig. 7 The SERS response of crystal violet (CV) molecules on NS-1 substrates shows a linear concentration dependence. (a) SERS spectrum of 10^{-12} M CV on 3 nM NS-1 substrate. (b) The variation of the SERS intensity as a function of CV concentration. The plotted SERS responses were collected for the 795 cm^{-1} peak under 785 nm laser excitation (166 µW).

The quantitative multiplexing ability of NS substrates was also studied by treating the 3nM NS-1 substrates with a mixture of 4-MBA and DBT. A characteristic vibrational mode of DBT at 1279 cm^{-1} was used along with the peak at 1077 cm^{-1} for 4-MBA to selectively identify the presence of each analyte on the SERS substrate. Fig. 7 shows that the presence of both 4-MBA and DBT can be clearly detected at a concentration as low as 1 pM.

Conclusions

We presented a novel SERS substrate for ultrasensitive quantitative chemical sensing applications. Our gold nanostar-based platform demonstrated commendable flexibility towards the analyte's identity, and was able to detect the presence of femtomolar amounts of analytes with low scattering cross section (MBA) as well as picomolar concentrations of analytes such as CV which lack pendant moieities that could enable covalent binding to the nanostructured gold surface. The modified synthetic protocol developed yielded gold nanostars bearing extremely sharp tips, which act as excellent SERS substrates. As a result, an outstanding overall SERS enhancement factor of 10^9 was obtained even in the absence of external quantum confinement effects. It also enabled both semi-quantitative, and qualitative multiplexed SERS-based sensing. In addition to these properties, the reproducibility and low cost fabrication, predictable surface coverage, and analyte-

binding effectiveness, render it a potential candidate for production and widespread distribution.

Acknowledgements
This work was supported by start up funds from Rutgers University and from the Rutgers Institute for Advanced Materials, Devices and Nanotechnology. The HIM work was supported by NSF grant DMR-1126468.

Notes and references
[a] Department of Materials Science and Engineering Rutgers University, 607 Taylor Road, Piscataway, New Jersey 08854, (USA).
[b] Institute for Advanced Materials Devices and Nanotechnology, 607 Taylor Road, Piscataway, New Jersey 08854, (USA).
[c] Department of Physics and Astronomy, Rutgers University, 136 Frelinghuysen Road, Piscataway, NJ 08854 (USA).

Electronic Supplementary Information (ESI) available: [details of any supplementary information available should be included here]. See DOI: 10.1039/b000000x/

1 M. Moskovits, *J. Raman Spectrosc.,* 2005, **36**, 485-496.
2 N. J. Halas, S. Lal, W. Chang, S. Link and P. Nordlander, *Chem. Rev.,* 2011, **111**, 3913-3961.
3 A. Campion and P. Kambhampati, *Chem. Soc. Rev.,* 1998, **27**, 241-250.
4 P. L. Stiles, J. A. Dieringer, N. C. Shah and R. P. Van Duyne, *Annu. Rev. Anal. Chem.,* 2008, **1**, 601-626.
5 E. C. Le Ru, E. Blackie, M. Meyer and P. G. Etchegoin, *J. Phys. Chem. C,* 2007, **111**, 13794-13803.
6 S. M. Nie and S. R. Emory, *Science,* 1997, **275**, 1102-1106.
7 K. Kneipp, *Phys. Rev. Lett.,* 1997, **78**, 1667-1670.
8 L. Fabris, M. Dante, T. Nguyen, J. B. -H. Tok and G. C. Bazan, *Adv. Funct. Mater.,* 2008, **18**, 2518-2525.
9 E. C. Le Ru and P. G. Etchegoin, *MRS Bull,* 2013, **38**, 631-640.
10 C. E. Talley, J. B. Jackson, C. Oubre, N. K. Grady, C. W. Hollars, S. M. Lane, T. R. Huser, P. Nordlander and N. J. Halas, *Nano Lett.,* 2005, **5**, 1569-1574.
11 L. Fabris, M. Schierhorn, M. Moskovits and G. C. Bazan, *Small,* 2010, **6**, 1550-1557.
12 A. S. D. S. Indrasekara, B. J. Paladini, D. J. Naczynski, V. Starovoytov, P. V. Moghe and L. Fabris, *Adv. Healthcare Mater.,* 2013, **2**, 1370-1376.
13 J. E. Millstone, S. Park, K. L. Shuford, L. Qin, G. C. Schatz and C. A. Mirkin, *J. Am. Chem. Soc.,* 2005, **127**, 5312-5313.
14 C. J. Murphy, T. K. Sau, A. M. Gole, C. J. Orendorff, J. Gao, L. Gou, S. E. Hunyadi and T. Li, *J Phys Chem B,* 2005, **109**, 13857-13870.
15 C. G. Khoury and T. Vo-Dinh, *J. Phys. Chem. C,* 2008, **112**, 18849-18859.
16 F. Hao, C. L. Nehl, J. H. Hafner and P. Nordlander, *Nano Lett.,* 2007, **7**, 729-732.
17 C. Hrelescu, T. K. Sau, A. L. Rogach, F. Jackel, G. Laurent, L. Douillard and F. Charra, *Nano Lett.,* 2011, **11**, 402-407.
18 C. Hrelescu, T. K. Sau, A. L. Rogach, F. Jackel and J. Feldmann, *Applied Physics Letters,* 2009, **94**, 153113-153113-3.
19 R. Alvarez-Puebla, L. M. Liz-Marzan and F. J. G. de Abajo, *J. Phys. Chem. Lett.,* 2010, **1**, 2428-2434.
20 L. Rodriguez-Lorenzo, R. A. Alvarez-Puebla, I. Pastoriza-Santos, S. Mazzucco, O. Stephan, M. Kociak, L. M. Liz-Marzan and F.J.G. de Abajo, *J. Am. Chem. Soc.,* 2009, **131**, 4616-4618.
21 H. Yuan, C. G. Khoury, H. Hwang, C. M. Wilson, G. A. Grant and T. Vo-Dinh, *Nanotechnology,* 2012, **23**, 075102.
22 L. Rodriguez-Lorenzo, R. A. Alvarez-Puebla, F. J. G. de Abajo and L. M. Liz-Marzan, *J. Phys. Chem. C,* 2010, **114**, 7336-7340.
23 E. N. Esenturk and A. R. H. Walker, *J. Raman Spectrosc.,* 2009, **40**, 86-91.
24 H. Yuan, Y. Liu, A. M. Fales, Y. L. Li, J. Liu and T. Vo-Dinh, *Anal. Chem.,* 2013, **85**, 208-212
25 Y. Pei, Z. Wang, S. Zong and Y. Cui, *J. Mater. Chem. B,* 2013, **1**, 3992-3998.
26 H. Yuan, A. M. Fales, C. G. Khoury, J. Liu and T. Vo-Dinh, *J. Raman Spectrosc.,* 2013, **44**, 234-239.
27 M. Jin, H. van Wolferen, H. Wormeester, A. van den Berg and E. T. Carlen, *Nanoscale,* 2012, **4**, 4712-4718.
28 S. L. Kleinman, B. Sharma, M. G. Blaber, A. Henry, N. Valley, R. G. Freeman, M. J. Natan, G. C. Schatz and R. P. Van Duyne, *J. Am. Chem. Soc.,* 2013, **135**, 301-308.
29 N. G. Greeneltch, M. G. Blaber, A. Henry, G. C. Schatz and R. P. Van Duyne, *Anal. Chem.,* 2013, **85**, 2297-2303.
30 B. Sharma, M. Fernanda Cardinal, S. L. Kleinman, N. G. Greeneltch, R. R. Frontiera, M. G. Blaber, G. C. Schatz and R. P. Van Duyne, *MRS Bull,* 2013, **38**, 615-624.
31 C. G. Khoury and T. Vo-Dinh, *J. Phys. Chem. C,* 2008, **112**, 18849-18859.
32 Y. Wang, A. E. DePrince, S. Gray K., X. Lin and M. Pelton, *J. Phys. Chem. Lett.,* 2010, **1**, 2692-2698.
33 L. Osinkina, T. Lohmuller, F. Jackel and J. Feldmann, *J. Phys. Chem. C,* 2013, **117**, 22198-22202.
34 P. N. Sisco and C. J. Murphy, *J Phys Chem A,* 2009, **113**, 3973-3978.
35 X. Hu, T. Wang, L. Wang and S. Dong, *J. Phys. Chem. C,* 2007, **111**, 6962-6969.
36 N. G. Bastus, J. Comenge and V. Puntes, *Langmuir,* 2011, **27**, 11098-11105.
37 A. Michota and J. Bukowska, *J. Raman Spectrosc.,* 2003, **34**, 21-25.
38 T. Chen, H. Wang, G. Chen, Y. Wang, Y. Feng, W. S. Teo, T. Wu and H. Chen, *ACS Nano,* 2010, **4**, 3087-3094.
39 P. C. Yohannan, V. H. Tresa, D Philip, *Spectrochim. Acta. A*, 2006, **65**, 802-804.
40 R. O Lezna, N. R. De Tacconi, S. A. Centeno, A. J. Arvia, *Langmuir*, 1991, **7**, 1241-1246.
41 P. S. Kumar, I. Pastoriza-Santos, B. Rodriguez-Gonzalez, F. J. G. de Abajo and L. M. Liz-Marzan, *Nanotechnology*, 2008, **19**, 015606.
42 J. Lee, B. Hua, S. Park, M. Ha, Y. Lee, Z. Fan and H. Ko, *Nanoscale*, 2014, **6**, 616-623.
43 R. A. Alvarez-Puebla, *J. Phys. Chem. Lett.*, 2012, **3**, 857-866.
44 A. C. Power, A. J. Betts and J. F. Cassidy, *Analyst*, 2011, **136**, 2794-2801.